J. Mech. Phys. Solids 146 (2021) 104212

Contents lists available at ScienceDirect

Journal of the Mechanics and Physics of Solids

journal homepage: www.elsevier.com/locate/jmps

Transient mechanics of slide-ring networks: A continuum model

Franck J. Vernerey *, Samuel Lamont

Department of Mechanical Engineering, Program of Materials Science and Engineering, University of Colorado, Boulder, USA

ARTICLE INFO

Keywords:
(B) Constitutive behavior
(B) Polymeric material
(B) Viscoelastic material
(C) Energy methods
(C) Probability and statistics
Transient network theory

ABSTRACT

Slide ring gels, developed from molecularly threaded polymer chains, have been getting increased attention for their unique modes of relaxation and toughness in the past ten years. While the methods of synthesis have become more sophisticated and efficient, theory has not kept up with experiments, and there exist many unexplained observations. In this paper, we develop a continuum-level model for slide ring gels based on thermodynamically consistent equations. We begin at the level of a single chain and perform statistical averaging to capture the unique molecular dynamics shown by polyrotaxane, the backbone chain of the network. We discover a unique dependence of relaxation on both level of strain and speed of deformation. We explain these properties quantitatively by assigning internal state variables that represent chain reptation and relative degree of chain-stretch and solve for their evolution during deformation.

1. Introduction

Polymer science is today undergoing unprecedented times in terms of developing high-precision soft materials with specialized functions. Particularly promising materials are based on the rotaxane template of interlocking macromolecules (Sauvage, 2017; Noda et al., 2014; Feringa, 2017), a large family of which have already been synthesized or studied for applications as broad as actuation (Goujon et al., 2017) and use as nano-valves (Boesten et al., 2010). A predominant feature of these topological constraints involves a unique source of configurational entropy sourced by threaded molecular rings. The effects of this entropy have been theorized to effect the response of both flexible chains (Baulin et al., 2005; Pinson et al., 2013) and stiff rods (Sevick and Williams, 2010). An important milestone in the production of topologically linked materials was the creation of slide-ring gels by using mobile rings as crosslinking junctions (Okumura and Ito, 2001). The tensile properties of the material were revealed to be exceptional (Bitoh et al., 2011), which Ito et al. associated to a pulley-effect (Ito, 2007). It was not until later that the entropic effects of mobile rings as described by Baulin et al. (2005), Pinson et al. (2013), Sevick and Williams (2010) were incorporated by Mayumi et al. into the modeling efforts to better understand the gels (Mayumi et al., 2012). Since then, studies on the molecular parameters (Kato et al., 2015), viscoelasticity (Kato et al., 2013), and fracture (Liu et al., 2017, 2019a) have been carried out on slide ring gels. Each of these experiments promotes the novelty and potential of these polymer networks for a myriad of uses; their unique dynamics provide an attractive framework for creating tunable materials with increasingly complex properties attributable to their topological nature. Progress on the modeling and theory side of this topic has not kept up with experiments, however, and there exists a large gap in our understanding of this material. This is a large hindrance to progress as the molecular parameters governing the response of slide ring gels are unaccounted for during synthesis, making it difficult for other researchers to replicate the results of those few groups who work on slide ring gels. Indeed, many methods of synthesizing slide-ring gels are now known (Hashidzume et al., 2019), but for the pool of research into slide ring gels to expand, understanding the molecular parameters involved in synthesis is crucial.

* Corresponding author.
E-mail address: franck.vernerey@colorado.edu (F.J. Vernerey).

https://doi.org/10.1016/j.jmps.2020.104212
Received 17 July 2020; Received in revised form 5 October 2020; Accepted 27 October 2020
Available online 1 November 2020
0022-5096/

The viscoelastic properties of most soft materials can be attributed to molecular rearrangement at small scales. Thus, viscoelastic polymers usually do not follow the classic affine model proposed by Flory and Rehner (1943), James and Guth (1943), Kuhn (1946), which assumes that chains are stretched as if attached to an elastic background. In fact, the unique form of reptation found in slide ring materials sharply contrast with this assumption — as crosslinked rings and chains move together within the network to dissipate energy. Some success has been made in describing non-affine behaviors by accounting for fluctuations as James (1947) did in his Phantom Network Model. Specifically, the Tube Model developed by Edwards (1967) was expanded into a non-affine model by Rubinstein and Panyukov (1997). This successfully explained some of the non-linearities associated with polymers, but failed to account for the possibility of slippage, which has been shown to be a significant mode of stress-relaxation in polymer melts (Doi and Edwards, 1978a). To account for this, these authors combined the work of Doi and Edwards (1978b) with the tube model and proposed the slip-tube model (Rubinstein and Panyukov, 2002). This was successful in combining the strengths of years of built-up work since the creation of soft materials, but its results suggested that a more novel approach might be necessary. Subsequently, De Gennes introduced the idea of chain reptation as a way of quantifying the rearrangement that occurs in polymer melts (de Gennes and Leger, 1982). It was thought that chains sliding within a polymer network could induce some level of relaxation due to the loosening of entanglements. The model still remains phenomenological as the observance of entanglements is difficult to quantify in many polymeric materials. The current state of theory for slide ring networks has not been updated to be in line with the state of experiments. Notably, a model posed by Ito in 2007 aimed to predict the typical 'S' shaped curve of a slide ring gel being pulled in tension (Ito, 2007). This model was able to predict a general qualitative trend of the gels, but could not predict some of the complexities associated with their response. The model was expanded on by Mayumi et al. in 2012 to incorporate a novel type of entropy derived from uncrosslinked mobile rings in the network (Mayumi et al., 2012). Although this model was capable of more sophisticated predictions, it has not been shown to accurately combine theory with experiments and bridge connections between the synthesis and resulting response of slide ring networks. Furthermore, a model that capable of predicting the transient response of slide ring networks has yet to be created. Such a model would be useful in not only explaining some of the complexities of slide ring materials, but also in aiding the development of smart materials based on similar structures.

The Transient Network Theory (TNT) has been used to describe networks that consist of chains that constantly detach and reattach over time (Tanaka and Edwards, 1992; Vernerey et al., 2017). In this situation, network relaxation occurs as highly stretched chains dissociate from its neighbors to reattach in a lower energy state. The dynamics displayed by slide ring gels are more similar to a slip-link model, which was used to describe chain sliding and relaxation as a result of chain entanglements (Ball et al., 1981). These entanglements were treated as creating a sort of reserve of monomers that could slide into the network when subject to certain stimuli. Slide ring gels behave in a similar way — chains slide through their fixed crosslinks by pulling on a reserve of monomers found in their dangling ends. In this way, it is not the network topology that changes over time, but rather the length of the chains between two crosslinks. In this paper, we formulate a model based on our previous works (Vernerey et al., 2017) that demonstrates the broad range of applications for TNT. Our objective is to develop a physically-motivated theoretical framework that can be used to associate key parameters involved in the synthesis of slide ring gels to their impact on the network's response. Our study is subdivided into two main contributions. We first develop a statistical model of a single polyrotaxane chain (Section 2) and analyze its behavior in different scenario (Section 3). This single-chain model is then used in Section 4 as a building block to construct a full network theory. Section 5 is then dedicated to exploring the model's prediction for the equilibrium and transient response of slide-ring gels in the light of existing experimental data. We finally conclude with a discussion in Section 6.

2. Transient response of a single polyrotaxane chain

Before we construct a full network model, it is necessary to develop a mathematical representation for the behavior of its elementary components, i.e. the polyrotaxane chains. These macromolecules can be represented by flexible chains threaded by slide rings that may or may not be crosslinked to the rest of the network (Fig. 1). The two end-chains are further capped with molecular "stoppers" that preclude the rings from dethreading. The mobile rings are able to slide along the chain and therefore do not constrain its motion. However, their thermal fluctuation creates a pseudo, one-directional osmotic pressure that results in chain pretension. By contrast, the constrained rings act as crosslinking points that restrict the motion of mid-segments, therefore governing the overall elasticity of the full chain. These crosslinks are nevertheless fundamentally mechanically different from covalent connections as they allow chain sliding, which eventually provides means for a network to relax its stored elastic energy. Our objective here is to describe the mechanical response of a single polyrotaxane chain when forces are applied to the crosslinked rings. For this, a chain is regarded as a series of N mid-segments, each separated by a crosslinked rings, and two end-segments (Fig. 1). For convenience, we introduce a numbering scheme where the mid-segments are indexed from 1 to N while the end-segment are represented by indices 0 and $N+1$. The $N+1$ crosslinked rings (or simply, crosslinkers) follow a similar numbering scheme such that the ith mid-segment is surrounded by links i and $i+1$. The kinematics of a polyrotaxane chain may be described by two main variables: (a) the position vectors $\boldsymbol{x}_i$ of each one of the crosslinkers and (b) the number n_i of monomers in each of its $N+2$ sub-chains (including the end segments). This may also be interpreted as the subchain's contour length $\ell_i = n_i b$ where b is the Kuhn length. As the chain is deformed, the motion of the crosslinkers induces a change in the end-to-end distance r_i of subchains such that:

$$r_i^2 = (\boldsymbol{x}_i - \boldsymbol{x}_{i-1}) \cdot (\boldsymbol{x}_i - \boldsymbol{x}_{i-1}) \tag{1}$$

Deformation also induces the sliding of monomers through the crosslinkers, which eventually changes the contour length $n_i b$ of sub-chains. To describe this process, we introduce the variable $\dot{\vartheta}_i$ that measures the rate at which monomers slide through the

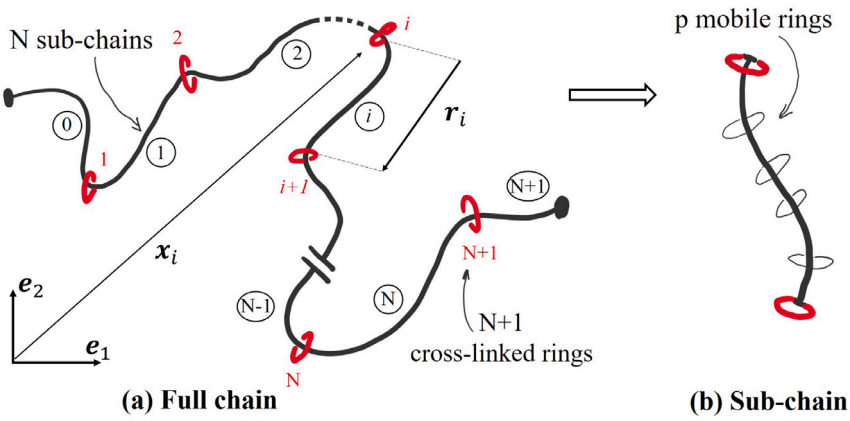

Fig. 1. A chain of polyrotaxane with N elastic mid-segments. The segments are numbered from left to right starting at $i = 0$, where the end segments correspond to $i = 0$ and $i = N + 1$. The crosslinked rings are numbered from 1 to $N + 1$. The coordinate of the ith crosslink and the end-to-end vector of the ith segment are indicated by $\boldsymbol{x}_i$ and $\boldsymbol{r}_i$, respectively. Here we do not show the mobile rings along the sub-segments for the sake of clarity.

i-th crosslinker. This variable should not be confused with the rate of change $\dot{n}_i$ in monomer number in segment i. In fact, the conservation of monomer along the chain imposes the relation:

$$\dot{n}_i = \dot{\vartheta}_{i+1} - \dot{\vartheta}_i \tag{2}$$

The transient response of a slide ring chain describes the out-of-equilibrium processes by which the sub-segments reorganize via chain reptation through the rings. In our approach, this translates into deriving governing equations for crosslinker variables $\boldsymbol{x}_i$ and ϑ_i as discussed next.

2.1. Entropic contributions

The response of a polyrotaxane chain is driven by the combined entropy of the flexible backbone, the mobile rings and their interactions. Following a similar approach as Pinson et al. (2013), we develop here a free energy functional that incorporates these various effects and their dependencies on the chain's physical properties. In the absence of enthalpic contributions, the free energy of a thermodynamical system is expressed as $\mathscr{F} = -TS$ where T is the absolute temperature and S is the entropy of its constituents, i.e. the chains and the rings.

Chain Entropy. For simplicity, we assume here that a flexible subchain follows Gaussian statistics. The probability for it to have an end-to-end distance r_i and contour length bn_i is given by $P(r_i, n_i) = [3/(2\pi n_i b^2)]^{3/2} \cdot exp(3r_i^2/2n_i b^2)$. Its entropy $S_i^{chain} = -klogP$ may thus be derived as:

$$S_i^{chain} = -\frac{3k}{2b^2}\left(\frac{r_i^2}{n_i}\right) - \frac{3k}{2}\log(n_i) \tag{3}$$

We note here that the assumption of Gaussian statistics is valid when the end-to-end distance is much smaller than the contour length ($r_i \ll n_i b$). We will see that this simplification has consequences on the response of a chain at high strains.

Ring Entropy. Mobile rings constantly rearrange their position on the contour length of the chain due to thermal fluctuations and therefore constitute a significant source of entropy (Mayumi et al., 2012). The entropy of rings is defined as $S_i^{ring} = klog\Omega$ where Ω is the number of configurations a mobile ring can take along a chain of contour length bn_i. The latter may easily be estimated with the binomial formula $\Omega = n_i!/(p!(n_i - p)!)$, while its logarithm can be simplified by Stirling's approximation in the limit of large n_i. This eventually yields the following form of the rings' entropy:

$$S_i^{ring} = k\left[n_i \log(n_i) - (n_i - p)\log(n_i - p)\right] \tag{4}$$

This formula can further be reduced to $S_i^{ring} = kp\log(n_i)$ if we assume $p \ll n_i$. It is however preferable to keep the above expression since the number n_i may be greatly reduced during chain deformation and n_i may approach p. This is particularly true in the dangling free ends of a chain as discussed later. The entropy being the sum of the chain and ring entropies, we obtain:

$$\mathscr{F} = kT\sum_{i=0}^{N+1}\left[\frac{3}{2b^2}\left(\frac{r_i^2}{n_i}\right) + \left(\frac{3}{2} - n_i\right)\log(n_i) + (n_i - p)\log(n_i - p)\right] \tag{5}$$

The summation is here taken over all subchains including both mid-segments and dangling ends.

2.2. Chain-ring friction

We hypothesize here that the transient response of a polyrotaxane chain is due to the time-dependent frictional behavior between the chain and the ring. When a ring undergoes a relative motion with respect to the chain, this motion is resisted by a tangential frictional force f_i^r that is proportional to the relative velocity $\dot{\vartheta}_i$. This allows us to write:

$$f_i^r = -\zeta \dot{\vartheta}_i \tag{6}$$

where ζ is the chain-ring friction coefficient. This process is associated with dissipation mechanisms with the following rate of energy loss ϕ at the level of the entire chain:

$$\phi = \sum_{i=1}^{N+1} \frac{\zeta}{2} \dot{\vartheta}_i^2 \tag{7}$$

By contrast to the free energy, the above dissipation potential is associated with kinetic processes. It is therefore representative of the non-equilibrium, rate-dependent response of the polyrotaxane chain.

2.3. Equations of motion

A Rayleigh functional can now be derived for the full chain that comprises contributions from the free energy, external forces and dissipation mechanisms. Following (Doi, 2013), this functional is expressed as the difference between the time variation of the total energy and the dissipation potential as

$$\mathscr{R} = \left(\dot{\mathscr{F}} + \phi\right) - \dot{\mathscr{W}} \tag{8}$$

where the work rate $\dot{\mathscr{W}}$ of external forces is here only due to forces $\boldsymbol{f}_i$ applied to crosslinking junctions. Thus, if $\dot{\boldsymbol{x}}_i$ is the velocity of the crosslinkers in the reference frame, we have:

$$\dot{\mathscr{W}} = \sum_{i=1}^{N+1} \boldsymbol{f}_i \cdot \dot{\boldsymbol{x}}_i \tag{9}$$

Using relationships (1) and (2), these equations can be solely expressed in terms of the crosslinker variables $\boldsymbol{x}_i$ and $\dot{\vartheta}_i$. The equations of motion are derived by minimizing the Rayleigh functional with respect to the generalized coordinates $\dot{\boldsymbol{X}} = \left(\dot{\boldsymbol{x}}_i, \dot{\vartheta}_i\right)$. This leads to the coupled system:

$$\dot{\mathscr{F}}_{,\dot{\boldsymbol{x}}_i} - \dot{\mathscr{W}}_{,\dot{\boldsymbol{x}}_i} = 0 \tag{10}$$

$$\dot{\mathscr{F}}_{,\dot{\vartheta}_i} + \zeta \dot{\vartheta}_i = 0 \tag{11}$$

Since this variation must vanish for any variations $\dot{\boldsymbol{x}}_i$ and $\dot{\vartheta}_i$ of the independent variables, we obtain a set of $N+1$ equations at crosslinking junctions:

$$[\boldsymbol{t}]_i = \boldsymbol{f} \tag{12}$$

$$[\pi]_i = \zeta \dot{\vartheta}_i \tag{13}$$

where the brackets are used to express a field discontinuity between two segments separated by crosslink i, i.e. $[a]_i = a_{i+1} - a_i$. We also introduced the tension vector $\boldsymbol{t}_i = \mathscr{F}_{,\boldsymbol{r}_i}$ and the osmotic pressure $\pi_i = \mathscr{F}_{,n_i}$ in chain i, respectively, as:

$$\boldsymbol{t}_i = \frac{3kT}{b^2} \frac{\boldsymbol{r}_i}{n_i} \quad \text{and} \quad \pi_i = \frac{3kT}{2} \left[g(n_i) - \left(\frac{r_i}{b n_i} \right)^2 \right] \tag{14}$$

where the function g was defined by:

$$g(n_i) = \frac{1}{n_i} + \frac{2}{3} \log\left(1 - \frac{p}{n_i}\right) \tag{15}$$

Eq. (12) can be recognized as a statement of the force balance at crosslink i. This equilibrium involves three forces: the externally applied force $\boldsymbol{f}_i$ and the elastic forces $\boldsymbol{t}_i$ and $\boldsymbol{t}_{i-1}$ of the two chains connected to the crosslinker (Fig. 2a). Since the end-segments are not subjected to external force, their tensions vanish, which yields the condition $\boldsymbol{t}_{N+1} = \boldsymbol{t}_0 = 0$. On the other hand, the second equation (13) involves the osmotic pressure π_i, which represents the driving force for monomer diffusion across crosslinkers. The equation therefore states that the difference in pressure between adjacent sub-chains drives the relative motion $\dot{\vartheta}_i$ of polymers through the ring that separates them.

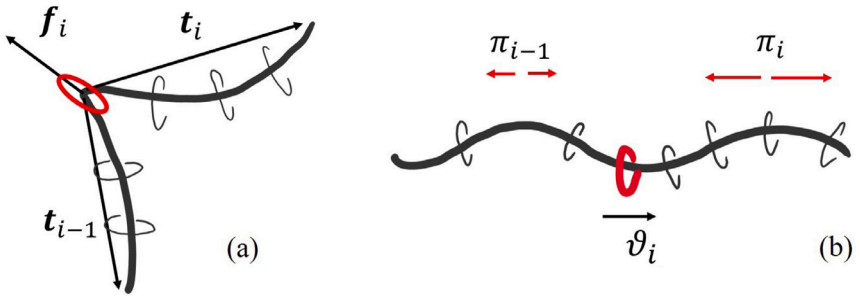

Fig. 2. (a) Force balance at a crosslinking junction along a continuous polyrotaxane chain. (b) Illustration of the osmotic pressure created by the presence of mobile rings threaded on a flexible chain. Monomers are driven to reptate across a crosslinker in order to decrease the pressure discontinuity between adjacent sub-segments.

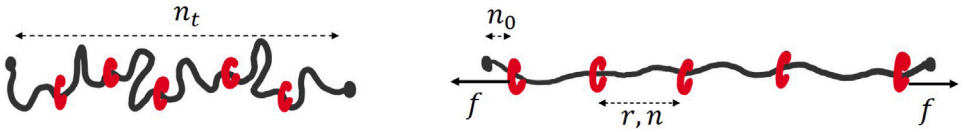

Fig. 3. Configurations of a polyrotaxane chain at rest and after the application of an external force $\boldsymbol{f}$ to its left and right crosslinkers.

2.4. Force free configuration, fast and slow loading

The above system of equations will next be used to explore the transient response of a polyrotaxane chain. It is however interesting to first explore a few simpler cases.

Force free configuration. If the chain is not subjected to any forces, the right end side of Eq. (12) vanishes and the chain tension becomes the same in all sub-segments. Since this force vanishes in the dangling ends, it also does in the mid-segment and $\boldsymbol{r}_i = 0$ everywhere. Eq. (13) then enforces that the osmotic pressure is equal in each sub-segment and equal to:

$$\pi_0 = \frac{3kT}{2} g(n) \tag{16}$$

where the number of monomer in a any sub-segment is $n = n_t/(N+2)$. When subjected to external forces, the rate dependent-response of a slide-ring chain should further be constrained between the slow and fast loading limits discussed below.

Slow loading (long-term equilibrium). In the limit of very slow loading (or deformation rate), the chain is able to reach its equilibrium state at all times. This means that the rates $\dot{\vartheta}_i$ and $\dot{\boldsymbol{x}}_i$ become negligible and the governing equations become:

$$[\boldsymbol{t}]_i = \boldsymbol{f} \tag{17}$$

$$[\pi]_i = 0 \tag{18}$$

In this situation, we see that the tangential force applied to the rings cannot be transferred to the chains. As a consequence, the discontinuity in chain tension only results from the normal component of the applied force. The applied tangential forces however have an effect on the segment's osmotic pressure, triggering sharp discontinuities at crosslinking junctions.

Fast loading (short-term equilibrium). When the deformation is applied very quickly, the chains do not have time to slide through the rings and (13) does not hold. Instead, it is replaced by the conditions that the monomer number remains constant in each segment, or:

$$[\boldsymbol{t}]_i = \boldsymbol{f} \tag{19}$$

$$\dot{\vartheta}_i = 0 \tag{20}$$

We note that this situation would also hold if the sliding crosslink was made covalent, i.e. they were unable to slide.

3. Mechanical behavior of a polyrotaxane chain

To illustrate the main trends exhibited by the model, we consider the response of a multi-segment polyrotaxane chain subjected to external forces applied to its crosslinkers. For clarity of the exposition, we concentrate on a chain whose crosslinkers are placed along a straight line (Fig. 3). This enables us to simplify the vectorial equation (12) by only considering its projection along the crosslinker's direction.

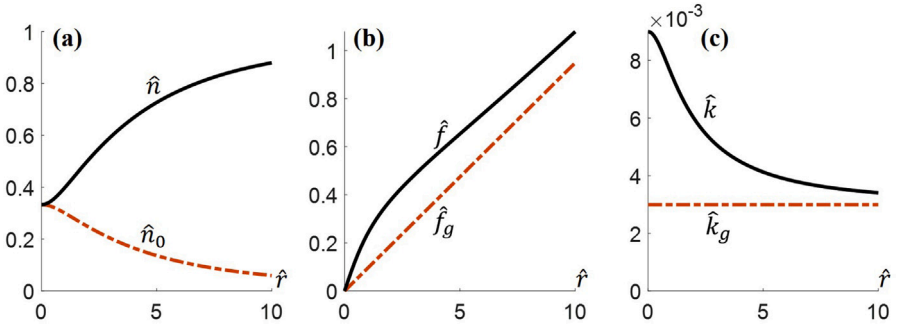

Fig. 4. (a) Equilibrium sliding of monomers in the middle (n) and end segments (n_0) in a single chain during stretching. Values normalized by chain length n_t for convenience. (b) Normalized force $\hat{f} = fb/kT$ response of a single chain plotted with the force response of a Gaussian chain f_g normalized in the same way. (c) Normalized chain stiffness $\hat{k} = kb^2/(kT)$ during stretching. As the monomers leave the dangling ends, the stiffness approaches that of a Gaussian chain (k_g). All plots against normalized end-to-end distance $\hat{r} = r/(b\sqrt{n_t})$.

3.1. Equilibrium of a single chain

We start by exploring the steady-state, equilibrium solution of a chain with $N+2$ segments and subjected to an external force $\boldsymbol{f}$ applied on the left and right crosslinkers as depicted in Fig. 3. At equilibrium, both the end-to-end distance r and number of monomers n are equal and constants in the mid-segments. In the dangling ends, the vanishing tension implies that $r_0 = r_{N+1} = 0$, while the monomer numbers $n_0 = n_{N+1}$ are constrained by the conservation equation $Nn + 2n_0 = n_t$. In the end, the system contains two unknown variables, r and n, that can be determined by equilibrium Eqs. (17) and (18). In our specific conditions, these equations simplify to:

$$N\left[\left(\frac{r}{bn}\right)^2 - g(n)\right] + g\left(\frac{n_t - Nn}{2}\right) = 0 \tag{21}$$

$$3r = nb\hat{f} \tag{22}$$

where the normalized force is $\hat{f} = fb/kT$. As discussed above, the resting state occurs when $r = 0$ and each chain has $n = n_0 = n_t/(N+2)$ monomers. As the chain is stretched, its response is constrained within the limit of this state and the point at which there are no monomers in the dangling ends, i.e. $n = n_t/N$.

Response of a 3-segment chain. We start by exploring the response of a 3-segment chain (one mid-segment and two dangling ends) with a ring to polymer ratio $\hat{p} = p/n_t = 1\%$ (Fig. 4). For clarity, results are presented in their non-dimensional form where the end-to-end vector of the mid-segment is normalized with respect to the resting length of the chain such that $\hat{r} = r/(b\sqrt{n_t})$. Fig. 4a shows how the chains slide through the rings as the end-to-end distance $\hat{r}$ increases from 0 to 10. During this process, the model predicts that the chain evolves from a configuration where all sub-chains are equally partitioned on each segment to a state where almost all monomers belong to the mid-segment ($n/n_t \approx 1$). Fig. 4b shows that the corresponding force/extension curve exhibits a large initial stiffness that gradually decreases to reach the stiffness of a regular flexible chain at large displacements. This observation is confirmed by comparing the system's stiffness (i.e. the derivative of the force with respect to the end-to-end distance of the mid-segment) to that of a flexible chain (Fig. 4c), where convergence is observed for a stretch ratio $\hat{r} \approx 10$. These general trends are in line (Fig. 5a) with those obtained earlier by Pinson et al. (2013) despite quantitative variations due to differences in the expressions of the chain and ring entropies.

Role of rings' inclusion ratio. When the chain is stretched, Fig. 5b shows that the addition of rings does not affect the general shape of the force–extension curve, but it does stiffens the chain at low deformation levels. In their non-dimensional form, these curves are only sensitive to the inclusion ratio $\hat{p} = p/n_t$ and remain unaffected by changing the chain length n_t. This implies that chain stiffness is inversely proportional to chain length as for a conventional flexible chain. The early chain stiffening with $\hat{p}$ with low inclusion ratio is due to the increased osmotic pressure, thus providing a threshold force for ring sliding at low forces. Once the force exceeds this ring-dependent threshold, the chain stiffness reverts to that of a conventional flexible chain with length bn_t.

Role of crosslink density. To complete our study of the chain's equilibrium response, we now depart from the 3-segment chain to explore the role of the number of mid-segments N (or equivalently, crosslink density). For illustration purposes, Fig. 6a&b show changes in force and stiffness for a chain with $N = 2$ and $N = 6$ mid-segments, respectively. We see that an increase in crosslink density is reflected by a rise in both chain force and chain stiffness. To quantitatively understand these observations, it is useful to realize that the chain response is constrained between two limits. On the one hand, the "no-sliding" limits corresponds to the situation where rings do not slide and the monomer number in each segment is $n_0 = n_t/(N+2)$. On the other hand, the "full-sliding" limit corresponds to the case where the chain reserve in the dangling ends has been emptied. In this case, the number of monomers in each mid-segment is $n = (n_t - 2p)/Nn_0$ as dictated by the logarithm in Eq. (15). Physically, this represents the minimum number of monomers required to thread the mobile rings contained in the dangling ends. In the limit of $p = 0$, the dangling ends can be

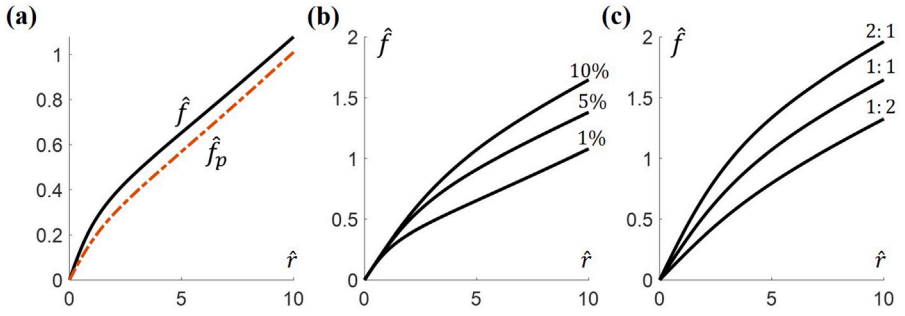

Fig. 5. (a) Normalized force $\hat{f} = fb/kT$ response of a single chain plotted alongside the model posed by Pinson et al. (2013). (b) The effect of varying inclusion ratio $\hat{p} = p/n_t$ during equilibrium stretching. (c) The effect of varying the ratio of mobile rings in the middle segments to the end segments during equilibrium stretching. All plots against normalized end-to-end distance $\hat{r} = r/(b\sqrt{n_t})$.

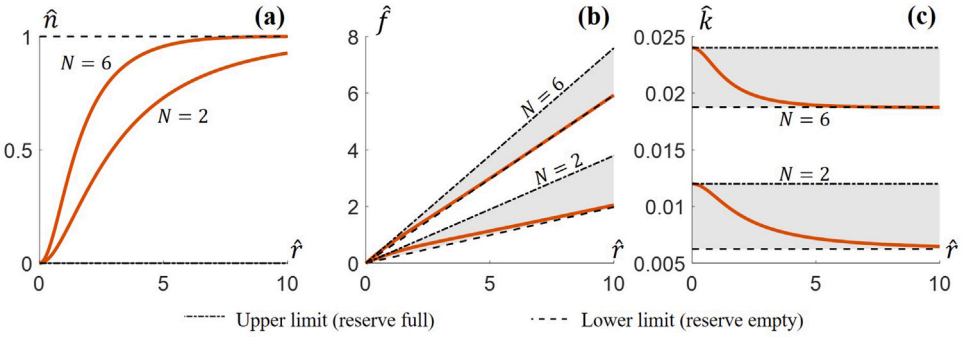

Fig. 6. The effect of varying crosslink density N on a single chain. (a) Normalized $\hat{n} = n(N+2)/n_t - 1$ versus normalized stretch $\hat{r} = r/b\sqrt{n_t}$. Chains with more segments approach their equilibrium value at a lower value of stretch. (b) Normalized force $\hat{f} = fb/kT$ response. Both chains are constrained to the limits corresponding to full and empty dangling ends. (c) Normalized chain stiffness $\hat{k} = kb^2/(kT)$. The response is constrained between an upper and lower bound as defined by $\hat{n} = 0, \hat{n} = 1$, corresponding to a full and empty reserve of monomers, respectively.

fully exhausted and the number of monomers in each mid-segment becomes $n = n_t/N$. This implies that the chain stiffness K should be bounded by:

$$\frac{3NkT}{n_t b^2} \leq K \leq \frac{3N(N+2)kT}{(n_t - 2p)b^2} \tag{23}$$

The transition between those two extreme cases is shown by simulations and reported in Fig. 6a. Consequences on the chain force and stiffness as depicted Fig. 6b&c, where it can clearly be seen that the response is constrained within the gray region representing the upper and lower bounds, thereby confirming their linear relation with crosslink density N.

3.2. Transient response

The transient response of the chain can be thought of as the process by which the chain transitions, in a rate dependent fashion, from the fast loading to the equilibrium solution discussed above. In the fast loading situation (dictated by Eq. (20)), the number of monomers in each subchain remains constant and equal to its initial value $n_i = n_0 = n_{N+1}$ throughout the deformation history. The end-to-end distance r in each segments is then determined by Eq. (22), where $n = n_t/(N+2)$. This is a trivial equation of a simple polymer chain stretched by a force F. In its dimensional form, this force is found to be:

$$f = \frac{3(N+2)kT}{n_t b^2} r \tag{24}$$

Force relaxation of a polyrotaxane chain. The force relaxation of a multi-segment polyrotaxane chain can be studied by prescribing the displacement of the two end rings to follow a very fast separation (relative to the relaxation time), that is later kept constant in time. The behavior of the chain is then given by evolution Eqs. (12) and (13) for the variables $(n_i(t), r_i(t))$ associated with each segment. By contrast to the equilibrium and fast solution, there is no simple uniform solution to these equations and the development of a numerical solution becomes necessary. In this work, we used a backward-Euler time integration scheme to solve the system of $2N$ coupled Eqs. (12) and (13) for a chain with $N+2$ segments (including the dangling ends). The numerical solution for a chain containing $N = 7$ mid-segment is provided in Fig. 7. For the sake of generality, we present results in terms of a normalized

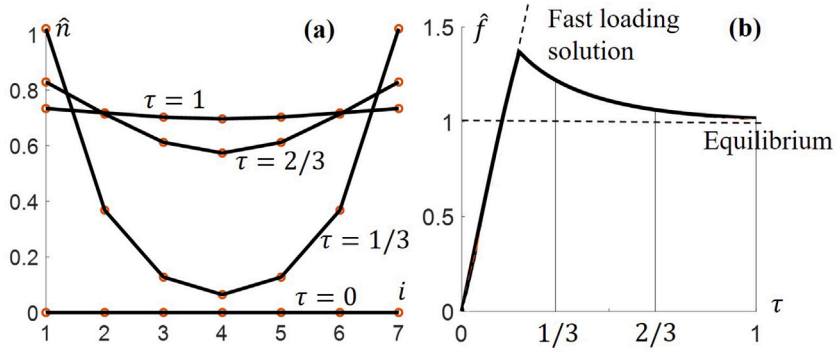

Fig. 7. Relaxation properties for a chain subject to stretch-rate $\dot{r}$ for a normalized time $\tau = 1/4$, where $\tau = 1$ is the full duration of the experiment, and then held constant. (a) Diffusion profile of the chain at different times during relaxation. (b) Normalized force $\hat{f} = f/f_{eq}$, where f_{eq} corresponds to the equilibrium force at the given stretch. As monomers flow into the middle segments, the force relaxes to its equilibrium value.

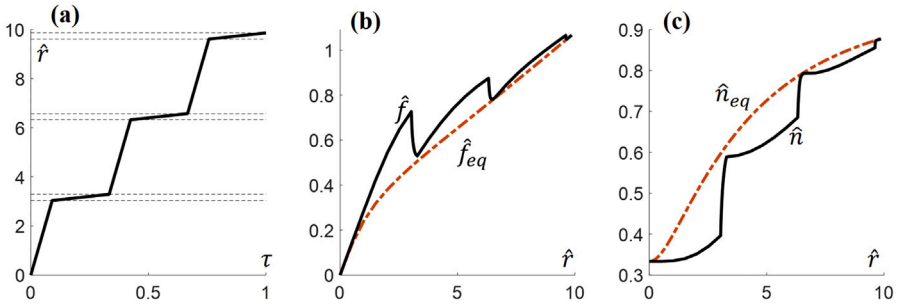

Fig. 8. Transient response of a single polyrotaxane chain with $N = 1$ middle segment. The chain is stretched periodically at a fast rate and a slow rate to allow intermittently for relaxation. (a) Loading profile normalized stretch $\hat{r} = r/b\sqrt{n_t}$ vs normalized time τ, where $\tau = 1$ corresponds to the total length of the experiment. (b) normalized force $\hat{f} = fb/kT$ response during stretching plotted with the equilibrium solution found using Eq. (22). (c) Normalized $\hat{n} = n/n_t$ plotted with the equilibrium solution found using Eq. (21).

time τ, where $\tau = 1$ is the full duration of the experiment. In this numerical experiment, the end rings are separated quickly by an amount $\hat{r} = 2/r_0$ and then held constant. Fig. 7a illustrates the change in monomer number in each sub-segment, represented by the non-dimensional number $\hat{n}_i = n_i/n_i(0) - 1$, where $n_i(0) = n_t/(N+2)$ is the initial number of monomers in a segment. We observe a diffusion-like profile where the chains closer to the extremities absorb new monomers from the dangling ends before the process propagates to the interior segments. Monomer diffusion via reptation proceeds until the osmotic pressure across all adjacent segments equilibrates. At this point, the solution reaches the equilibrium state described in Section 3.1. Fig. 7b shows the corresponding force-time profile, where it is clear that the chain response transitions from the fast-loading to the equilibrium solution at long times. For generality, results are presented in terms of a force $\hat{f} = 3fb(N+2)/n_t kT$ that is normalized by its equilibrium value. We clearly see that the rate dependent process of chain sliding through the rings yields a force relaxation with a characteristic time that scales linearly with the friction coefficient ζ. The dependency of this rate on other parameters are explored later in this section.

Relaxation decreases with stretch level. A particularly interesting behavior of polyrotaxane chains is that the amount of force relaxation is dependent on the level of applied stretch. To illustrate this feature, let us consider the simple case of a three-segment chain (i.e. $N = 1$) and apply a series of fast stretches on its two end-rings, separated in time by very slow separation rate in order to allow force relaxation. Fig. 8a provides the details of the stretch history that comprises a pseudo-stress relaxation at three different levels of stretches $\hat{r} = 3.3$, 6.6 and 10. The corresponding stretch-force response (Fig. 8b) depicts a stiff chain response that follows the fast solution during the quick loading stage and a subsequent stress relaxation to the equilibrium solution during the slow loading stage. The magnitude of this relaxation however decreases significantly with stretch until it is hardly perceptible. The cause of this phenomenon is the strain-induced exhaustion of the chain reserve from the dangling ends as shown in Fig. 8c. This clear correspondence between the amount of chain reserve and the magnitude of stress relaxation is characteristic of this particular type of sliding crosslinks.

Role of chain structure on relaxation time. We have seen that the friction coefficient ζ is the main parameter that governs the relaxation rate of the chain. Other parameters such as crosslink density N, inclusion ratio $\hat{p} = p/n_t$ and chain length n_t are however expected to play an indirect role, owning to their effect on the osmotic pressure π_i which eventually governs the sliding process. To explore these effects, we considered the single relaxation test presented in Fig. 7 for a reference chain characterized by $N = 5$, $p = 10$

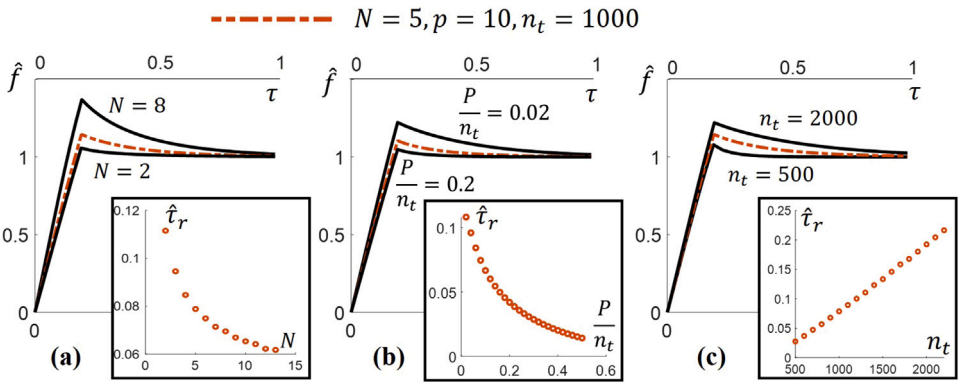

Fig. 9. The effect of molecular parameters on relaxation time $\hat{\tau}_r$. Normalized force $\hat{f} = f/f_{eq}$ vs normalized time τ, where $\tau = 1$ corresponds to the total duration of the experiment. Relaxation time is found by fitting an exponential decay function for varying (a) crosslink density N (b) inclusion ratio $\hat{p}$ and (c) chain length n_t.

and $n_t = 1000$. We then independently varied the three above parameters about this reference point to quantify their role on force relaxation. We particularly focused on the relaxation time as determined by fitting an exponential decay function $\hat{f} - f_0 = Aexp(t/\tau_r)$, where the characteristic time τ_r was our fitting parameter. These results are presented in Fig. 9. Generally, they show that relaxation time increases linearly with chain length n_t, but decreases in a nonlinear fashion with crosslink density N and inclusion ratio $\hat{p}$. Although it is beyond the scope of this work, this parametric study motivates future investigations that would lead to the derivation of scaling laws relating molecular design and relaxation time of polyrotaxane chains.

4. Transient response of slide-ring networks

The model of a single polyrotaxane chain provides a solid basis to study the mechanics of a full network. The bridge between the molecular and macroscopic scale is however not trivial as it not only depends on the response of each chain, but also on their interactions. In this section, we propose to simplify the problem by taking a statistical approach that allows us to consider the crosslinkers as part of a continuum whose deformation follows the macroscopic deformation on average.

4.1. Statistical description of slide-rings networks

The first step in constructing a continuum theory is to derive an averaged version of the free energy functional shown in (5). With this in mind, it is first useful to note that the elastic energy of a mid-chain is entirely described by its normalized end-to-end vector

$$\lambda = \frac{\boldsymbol{r}}{b\sqrt{n}} \tag{25}$$

This vector is usually best characterized by its magnitude λ and direction angles θ and ϕ in a spherical coordinate system. At the network level, the accurate knowledge of each subchain is typically difficult to obtain due to their high number. Instead, we take a statistical approach where the number of mid-segment is so large that it can be described by continuous functions of λ, θ and ϕ. The conformation space is here defined as the space defined by $\lambda \in \mathbf{R}^+$, $\theta \in [0, 2\pi]$, $\phi \in [0, \pi]$. In this space, an infinitesimal volume $d\Omega = \sin\theta d\lambda d\theta d\phi$ defines a small region that can be explored by chains within all possibilities of conformations. The infinitesimal probability dP of finding a mid-chain in a small volume centered around the value λ is provided by the product $dP = p(\lambda)d\Omega$, where the quantity $p(\lambda)$ measures the probability density around λ. As shown in Fig. 10, this probability density function (or *pdf*) provides a statistical description of the conformation of the entire population of mid-segments in the network. By definition, the integration of this function over the entire space Ω verifies:

$$\int_\Omega p(\lambda)d\Omega = 1 \tag{26}$$

Importantly, this function will enable us to connect the mechanics of single chains to the full network by defining an average operator. For this, let us consider an arbitrary function $f(\lambda)$ that locally describes a physical quantity associated with a chain in conformation λ. The average of this quantity over the entire network is then assessed by the operator $\langle\cdot\rangle$ such that:

$$\langle f \rangle = \int_\Omega p(\lambda) f(\lambda) d\Omega \tag{27}$$

Using these concepts, let us now express the average free energy of a network made by a population of polyrotaxane chains with N mid-segments. At this level, it is sufficient to describe the number of monomers in a mid-chain (characterized by its index i) as

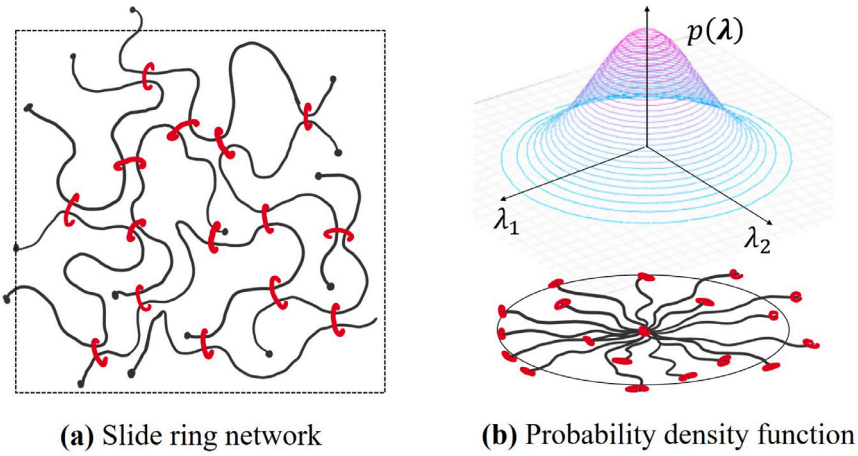

Fig. 10. (a) Illustration of a network of flexible chains crosslinked by slide rings (mobile rings not shown) and (b) corresponding probability density function (*pdf*) of the normalized end-to-end vectors λ of its mid-chains. This function captures the density of chains with specific lengths and orientations in the networks. In its stress-free state, the network is isotropic and the *pdf* exhibits directional symmetry.

its chain-average $n = \sum n_i/N$. For convenience, this variable is redefined in a nondimensional form as:

$$\alpha = n/n_0 \tag{28}$$

where $n_0 = n_t/(N+2)$ is the average number of monomers in a middle segment in a stress-free configuration. This nondimensional parameter captures the time-dependency of monomers sliding within a chain. When $\alpha = 1$, the monomers are equally distributed in the mid-segment and the dangling ends. By contrast, when $\alpha = (N+2)/N$, the monomer reserve in the dangling ends is fully exhausted. Using the average operation (27), the mean free energy $\langle \mathscr{F} \rangle$ can be directly derived from Eq. (5) as:

$$\langle \mathscr{F} \rangle = NkT \left[\frac{3}{2}\langle \lambda^2 \rangle + h(n_0\alpha) + \frac{2}{N} h\left(\frac{n_t - N n_0 \alpha}{2} \right) \right] \tag{29}$$

where the function h has the form:

$$h(n) = (3/2 - n)\log(n) + (n - p)\log(n - p) \tag{30}$$

Thus, if we consider a network whose density of full polyrotaxane chains is c (measured in moles of chains per unit volume), the free energy density becomes $\psi = c\langle \mathscr{F} \rangle$. This yields the energy functional ψ_N for the full network:

$$\psi_N(p(\lambda), \alpha) = cNkT \left[\frac{3}{2}\langle \lambda^2 \rangle + h(n_0\alpha) + \frac{2}{N} h\left(\frac{n_t - N n_0 \alpha}{2} \right) \right] \tag{31}$$

This expression is implicitly a function of the probability function $p(\lambda)$ (via the average operator $\langle \lambda^2 \rangle$) and is therefore not straightforward to use as a continuum model. To resolve this issue, we next introduce a macroscopic deformation measure that can be used to assess the average stretch of a subchain due to the overall distortion of the network and chain reptation (see Fig. 10).

4.2. Network deformation and chain stretch

The macroscopic deformation of an elastic solid is generally described by the deformation gradient $\boldsymbol{F} = \partial \boldsymbol{x}/\partial \boldsymbol{X}$ where $\boldsymbol{X}$ and $\boldsymbol{x}$ are the position coordinate of a continuum point in its reference and current configuration. This tensor captures both the distortion and the rotation of an elementary material volume. In the present study, we assume an incompressible network, imposing that the network's volumetric deformation $J = det(\boldsymbol{F})$ verifies

$$det(\boldsymbol{F}) = 1 \tag{32}$$

at all times. Furthermore, since the rotation of a material point is not associated with any stored elastic storage, it is more appropriate to use the Finger deformation tensor $\boldsymbol{B} = \boldsymbol{F} \cdot \boldsymbol{F}^T$ as a true measure of the solid's elastic distortion. When the solid is inelastic – it is the case for slide ring networks – this concept is no longer valid and a new definition of the elastic distortion is necessary.

4.2.1. The chain conformation tensor

The transient network theory (TNT) (Vernerey et al., 2017) provides a convenient approach to generalize the definition of the average elastic deformation of chains in the network via the averaging operation:

$$\boldsymbol{B} = \langle \lambda \otimes \lambda \rangle \tag{33}$$

where the stretch tensor of a chain was defined in Eq. (25). The conformation tensor $\boldsymbol{B}$ provides a directional representation of the squared stretch of chains in the network. Like the Finger deformation, it is represented by a symmetric tensor that can be written using a spectral decomposition in terms of its principal values and directions. The conformation tensor can therefore be graphically depicted as an ellipsoid with axes whose lengths and directions correspond to its eigenvalues and eigenvectors, respectively. In a stress-free state, the average stretch is equal to 1 in all directions and $\boldsymbol{B} = \boldsymbol{I}$, where $\boldsymbol{I}$ is the identity matrix (i.e, it can be represented as the unit circle in two-dimension).

4.2.2. Evolution of chain conformation

We have seen earlier that the elastic stretch of a chain changes over time due to the combination of externally applied forces and its reptation through the crosslinks. These mechanisms can readily be expressed through the evolution of the probability density function $p(\lambda)$:

$$\dot{p} = -\frac{\partial}{\partial \lambda}(p\dot{\lambda}) \tag{34}$$

where a superimposed dot denotes a material time derivative. To estimate the rate of chain stretch $\dot{\lambda}$, let us first suppose that the network is subjected to an overall rate of deformation characterized by the velocity gradient $\boldsymbol{L} = \dot{\boldsymbol{F}} \cdot \boldsymbol{F}^{-1}$. Now, if one assumes that the crosslinkers deform affinely with the rest of the network, the end-to-end vector of a chain follows the linear transformation $\dot{\boldsymbol{r}} = \boldsymbol{L}\boldsymbol{r}$. Using the definition of the stretch ratio (25) and the chain reserve α in (28), one finds that:

$$\dot{\lambda} = \left(\boldsymbol{L} - \frac{\dot{\alpha}}{2\alpha}\boldsymbol{I}\right)\lambda \tag{35}$$

Using this expression in (34), we find an evolution equation for the probability density function:

$$\frac{Dp}{Dt} = -\boldsymbol{L} : (\nabla p \otimes \lambda) + \frac{\dot{\alpha}}{2\alpha}(\nabla p \cdot \lambda + 3p) \tag{36}$$

where the gradient operator ∇ represents derivatives with respect to λ. This equation may be thought of as a type of Fokker–Planck equation for a chain population whose crosslinkers deform affinely with the velocity gradient $\boldsymbol{L}$ and slide through the crosslinkers at a rate $\dot{\alpha}$. Multiplying this equation by the quantity $\lambda \otimes \lambda$ and integrating over the chain configurational space Ω finally leads to the following evolution equation for the conformation tensor:

$$\dot{\boldsymbol{B}} = \boldsymbol{L}\boldsymbol{B} + \boldsymbol{B}\boldsymbol{L}^T - \frac{\dot{\alpha}}{\alpha}\boldsymbol{B} \tag{37}$$

where we used the incompressibility condition in its rate form $Tr(\boldsymbol{L}) = 0$. As expected, the overall chain stretch increases with the application of a velocity gradient $\boldsymbol{L}$ (first two terms) and generally decreases with chain reptation through the crosslinkers (last term). We note that if chain reptation ceases ($\dot{\alpha} = 0$), Eq. (37) can readily be integrated to find $\boldsymbol{B} = \boldsymbol{F}\boldsymbol{F}^T$. In other words, the conformation tensor degenerates to the Finger deformation tensor if the network is fully elastic (no sliding).

Conveniently, the average $\langle\lambda^2\rangle$ appearing in Eq. (31) can be expressed in terms of $\boldsymbol{B}$ by realizing that $\langle\lambda^2\rangle = Tr(\boldsymbol{B})$. This allows us to rewrite the network's free energy in the form:

$$\psi(\boldsymbol{B}, \alpha) = cNkT\left[\frac{1}{2}\mathrm{Tr}(\boldsymbol{B}) + h(n_0\alpha) + \frac{2}{N}h\left(\frac{n_t - Nn_0\alpha}{2}\right)\right] + \Pi(\det(\boldsymbol{F}) - 1) \tag{38}$$

where the last term enable us to enforce the incompressibility constraints via the Lagrange multiplier method. The Lagrange multiplier Π may here be interpreted as the hydrostatic pressure necessary to preserve the network's original volume during deformation. The free energy (38) is now only a function of two "macroscopic" internal variables $\boldsymbol{B}$ and α. The final step is to determine a set of thermodynamically consistent evolution laws for these variables and define their relation to network stress.

4.3. Thermodynamically admissible constitutive relations

The network stress $\boldsymbol{\sigma}$ is a macroscopic manifestation of the combined tension in sub-chains averaged over a cross-sectional area. From an energetic point of view, $\boldsymbol{\sigma}$ is also the force conjugate to the velocity gradient, and therefore, the rate of work of internal forces (per unit volume) can be assessed by the tensor contraction $\mathscr{W}^{int} = \boldsymbol{\sigma} : \boldsymbol{L}$. In the absence of heat flux or temperature change, the second law of thermodynamics enforces that

$$\mathscr{D} = \boldsymbol{\sigma} : \boldsymbol{L} - \dot{\psi} \geq 0 \tag{39}$$

where $\mathscr{D}$ is the energy dissipation per unit volume and ψ is the free energy density expressed in Eq. (38). Using the chain rule and Eq. (37), the material time derivative $\dot{\psi}$ of the free energy takes the form:

$$\dot{\psi} = \left(2\boldsymbol{B}\frac{\partial\psi}{\partial\boldsymbol{B}} + \Pi\boldsymbol{I}\right) : \boldsymbol{L} + \left(\frac{\partial\psi}{\partial\alpha} - \frac{1}{\alpha}\frac{\partial\psi}{\partial\boldsymbol{B}} : \boldsymbol{B}\right)\dot{\alpha} \tag{40}$$

$$= (cNkT\boldsymbol{B} + \Pi\boldsymbol{I}) : \boldsymbol{L} + \pi\dot{\alpha} \tag{41}$$

where we introduced the network version of the mobile rings' osmotic pressure π as:

$$\pi = \frac{3cNkTn_0}{2}\left(g(n_0\alpha) - g\left(\frac{n_t - Nn_0\alpha}{2}\right) - \frac{2Tr(\boldsymbol{B})}{3n_0\alpha}\right) \tag{42}$$

where the function $g(n) = dh/dn$ was already defined at the chain level in Eq. (15). We rewrite it here for ease of legibility.

$$g(n) = \frac{1}{n} + \frac{2}{3}\log\left(1 - \frac{p}{n}\right) \tag{43}$$

We note that these expressions can be interpreted as averaged, network versions of those already introduced for a single chain in Eqs. (14). Substituting expression (41) into inequality (39) finally leads to the Clausius–Duhem inequality for slide-ring networks:

$$(\boldsymbol{\sigma} - cNkT\boldsymbol{B} - \Pi\boldsymbol{I}) : \boldsymbol{L} - \pi\dot{\alpha} \geq 0 \tag{44}$$

Assuming that there are no dissipation mechanisms other than chain sliding, the first term vanishes, leading to:

$$\boldsymbol{\sigma} = cNkT\boldsymbol{B} + \Pi\boldsymbol{I} \tag{45}$$

While this equation seems to be identical to that defining an incompressible elastic Neo-Hookean solid, the conformation tensor $\boldsymbol{B}$ here represents the elastic deformation of chains and does relax over time due to chain reptation through the rings (see Eq. (37)). The Cauchy stress is thus expected to relax linearly with the conformation tensor until the network reaches its equilibrium. In these conditions, the dissipation becomes:

$$\mathscr{D} = -\pi\dot{\alpha} \geq 0 \tag{46}$$

This gives a necessary condition for the development of a constitutive relation linking the continuum level driving force π and the rate of ring reptation $\dot{\alpha}$. One of the simplest forms that verifies equation (46) is:

$$\dot{\alpha} = -\pi/\xi \tag{47}$$

where ξ is a positive friction coefficient, representing the resistance to monomer reptation at the continuum level. It may be interpreted as the continuum version of expression (13). Substituting this constitutive relation into Eq. (46) shows that the dissipation can be expressed as a harmonic function of the driving force and thus remains positive at all time. To complete the model, we finally substitute equation (47) into (37) and obtain:

$$\dot{\boldsymbol{B}} = \boldsymbol{L}\boldsymbol{B} + \boldsymbol{B}\boldsymbol{L}^T + \frac{\pi}{\xi\alpha}\boldsymbol{B} \tag{48}$$

Eqs. (45) and (48) therefore constitute the final form of the stress/deformation relationship for our slide ring network.

4.4. Alternative form of the theory

The form of the above theoretical framework closely follow that of the TNT (Vernerey et al., 2017). A slightly different form may alternatively be obtained by substituting Eq. (25) into (33) to find that $\boldsymbol{B} = \langle \boldsymbol{r} \otimes \boldsymbol{r}\rangle / nb^2$. Further using the affine assumption $\boldsymbol{r} = \boldsymbol{F}\boldsymbol{R}$, we find that $\langle \boldsymbol{r} \otimes \boldsymbol{r}\rangle = (\boldsymbol{F}\boldsymbol{F}^T)\langle \boldsymbol{R} \otimes \boldsymbol{R}\rangle$. Realizing that for an isotropic network with original chain length $n_0 = n_t/(N+2)$, we have $\langle \boldsymbol{R} \otimes \boldsymbol{R}\rangle = n_0 b^2 \boldsymbol{I}$, the conformation tensor can directly be expressed in terms of α as follows:

$$\boldsymbol{B} = \left(\boldsymbol{F}\boldsymbol{F}^T\right)/\alpha \tag{49}$$

The network (Cauchy) stress in the slide-ring network is then

$$\boldsymbol{\sigma} = G\boldsymbol{F}\boldsymbol{F}^T + \Pi\boldsymbol{I} \quad \text{where} \quad G = ckTN/\alpha \tag{50}$$

is the shear modulus of the network. In other words, the stress can be directly determined from the knowledge of the deformation gradient $\boldsymbol{F}$ and the internal variable $\alpha(t)$. In this version of the theory, the latter is directly determined by integrating equation (47) over time. One advantage of this form is that one can clearly see that the equilibrium and transient response of a transient network is constrained between two bounds that correspond to the extreme limits of α discussed in the previous sections. For the upper-bound, the average number of monomers in a mid-segment does not change during deformation and $\alpha = 1$. On the other hand, the lower-bound corresponds to the case where the monomer reserve from the dangling ends is emptied. Following the single-chain case, this is physically limited by the mobile rings threaded on the dangling ends. The lower bound is thus given by $\alpha = (N+2)(n_t - 2p)/Nn_t$. The effective shear modulus of the network is therefore constrained between:

$$\frac{ckTN^2 n_t}{(N+2)(n_t - 2p)} \leq G \leq ckTN \tag{51}$$

5. Model analysis and illustrations

In this section, we explore the model's predictions in the case of a uniaxial tensile test of a slide ring gel. Similar to Section 3, we first concentrate on time independent behavior in order to better orient the subsequent discussion of the transient response. The uniaxial tension of a specimen is simulated by subjecting it to a uniform deformation gradient:

$$\boldsymbol{F}(t) = Diag(1 + \epsilon(t), 1/\sqrt{1+\epsilon(t)}, 1/\sqrt{1+\epsilon(t)}) \tag{52}$$

in an orthonormal coordinate systems with axes in the principal directions. Here, $\epsilon(t)$ is the axial strain, while the lateral components ensure that the deformation is volume preserving (i.e. $det(\boldsymbol{F}) = 1$). Using this expression in Eq. (50) and enforcing a zero-stress in lateral directions, we find that the axial stress $\sigma = \sigma_{11}$ is:

$$\sigma(t) = \frac{ckTN}{\alpha(t)}\left((1+\epsilon(t))^2 - \frac{1}{1+\epsilon(t)}\right) \tag{53}$$

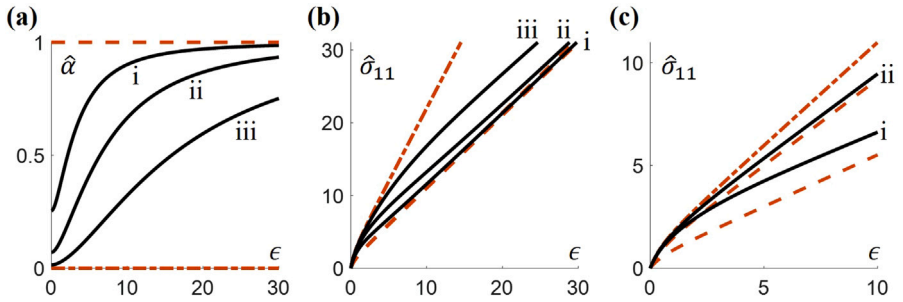

Fig. 11. Equilibrium force response for varying model parameters. (a) and (b) reflect the response of networks with inclusion ratio $\hat{p}/n_t$= 0.1%, 1%, and 10% for networks i, ii, and iii. (a) The sliding exhibited by the networks (illustrated with continuum variable α) with its upper and lower bounds. We normalize α bt its upper and lower bounds such that it varies between 0 and 1. (b) The resulting normalized stress $\hat{\sigma}_{11} = \sigma_{11}/ckT$ with its soft and stiff solutions as bounds. (c) Normalized stress $\hat{\sigma}_{11} = \sigma_{11}/NckT$ plots for high ($N = 6$) and low ($N = 2$) crosslinker densities (i and ii, respectively). Dashed lines represent the expected response of the network with constant $\hat{\alpha}$ at each of its extremes (corresponding to a full and empty reserve of monomers, respectively.).

5.1. Equilibrium response

The equilibrium network response occurs when the sliding rate vanishes ($\dot{\alpha} = 0$) which, according to Eq. (47) corresponds to a vanishing osmotic pressure π. We can therefore evaluate the variable α by numerically finding the root of Eq. (42)) and compute the corresponding stress from (50). With this approach, let us explore the network response with changing inclusion ratio $\hat{p} = p/n_t$ and crosslink density $\rho = cN$ (i.e. number of crosslinks per network volume). For illustration purposes, Fig. 11 shows plots of chain reptation α and stress σ as a function of strain ϵ for three distinct inclusion ratios and two crosslinker densities. As expected, results show that the stress–strain response originally follows the upper-bound (stiff) solution to eventually converge to its lower bound (soft) counterpart when the deformation is large. We can also observe that this change in network stiffness is due to chain reptation until the chain reserve in the dangling ends is fully exhausted (i.e. when $\hat{\alpha}$ goes to 1). Interestingly, as the inclusion ratio is increased, chain reptation is delayed to larger stress, and the network follows the stiff solution for a larger range of deformation. Indeed, as suggested in the previous sections, an increased number of mobile rings prevents the sliding of monomers and thus maintains the stress closer to the stiff solution. This is reflected in the small change in α shown in Fig. 11a for the largest inclusion ratio (iii). Similar trends were observed experimentally by Ito (2012) and Kato et al. (2015).

The crosslink density ρ is a common means of adjusting the stiffness of a polymer network. For a slide-ring network, ρ can be changed by varying the average number of segments in a single chain (N) or simply varying the chain concentration c. While the stress only has a linear dependence on c, it decreases with N due to its dependence on $N/(N+2)$ (see Eq. (49)). Fig. 11c illustrates this effect, where it can be observed that the difference between the lower and upper bounds fades as N increases from 2 to 6 (the stress is further normalized by N to illustrate this). This represents the physical limitations of the network; a chain with more crosslinkers will have fewer monomers in the dangling ends in the stress-free state and will thus display less relaxation. By varying the concentration of polyrotaxane used, Jiang et al. discovered similar results (Jiang et al., 2018).

5.2. Transient response

Let us now explore the theoretical predictions of the time-dependent response of the network by simulating classical rheological experiments. In this case, the driving force for chain reptation is found by solving equation (42), while the resulting sliding is found from Eq. (47). Under a given strain rate, this enables us to determine the time evolution of $\mathbf{B}$ and α. We use an iterative solving scheme that calculates $\dot{\alpha}$ and $\dot{\mathbf{B}}$ at discrete timesteps and updates their values at a small change in time Δt. The stress of the network is then found from Eq. (50). For illustration purposes, we normalize the parameter α such that it varies between 0 and 1. According to the bounds in (49), the normalization formula becomes $\hat{\alpha} = (\alpha - 1)Nn_t/2(n_t - 4p - 2N)$. To comply more closely with experiments reported in the literature, we use a constant loading velocity in the simulations. The engineering strain ϵ is therefore a linear function of time:

$$\epsilon = vt/\ell_0 \tag{54}$$

where ℓ_0 is the reference length of the specimen and v is the applied velocity.

5.2.1. The amount of relaxation is dependent on stretch

The time dependent response of the gel is first assessed by simulating a standard stress relaxation test. In this numerical experiment, the network is successively stretched (quickly) to a fixed value of strain $\Delta\epsilon = 3$ and then allowed to relax by holding the deformation. The normalized loading velocity $\hat{v} = vn_t^2/\xi$ is taken to be high enough ($\hat{v} = 1$) so that stress relaxation does not occur during the stretching phase. As expected, $\hat{\alpha}$ varies between its bounds and increases as the network relaxes. The changes in α are coupled with stress relaxation as shown in Fig. 12b and c. Interestingly, even though the network is stretched by the same amount at each step, we see a higher amount of relaxation in the second step. This is explained by the 'S' shaped α vs ϵ curve displayed in

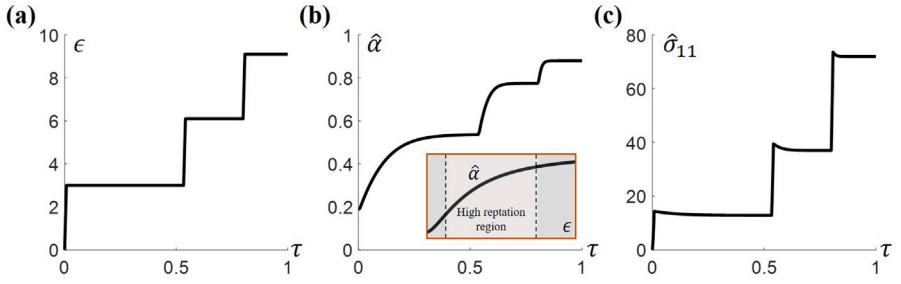

Fig. 12. (a) Loading profile. The network is rapidly stretched at a constant velocity and then allowed to relax for a time $\tau = 1/3$, where $\tau = 1$ is the total length of the experiment. (b) The change in α vs τ. We see the largest change at the largest stretch ratio. (c) Normalized stress $\sigma_{11}/cNkT$ vs τ. The parameters of the network are $p = 10, N = 5$, and $n_t = 1000$.

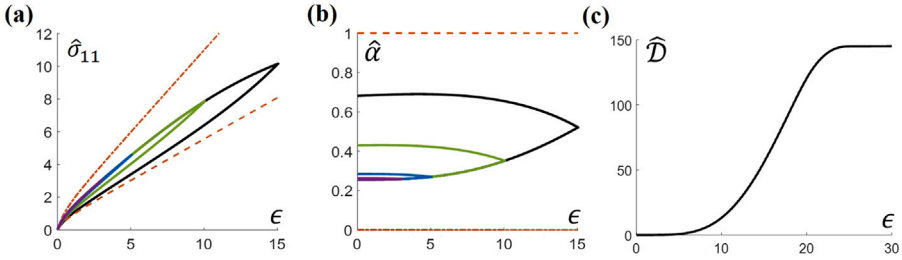

Fig. 13. Cyclic loading experiment for different stretch ratios. (a) Normalized stress $\sigma_{11}/cNkT$. (b) α vs strain ϵ. Dashed bounds are given as the soft and stiff solutions derived in previous sections, corresponding to a full and empty reserve. (c) Normalized energy dissipation $\hat{\mathscr{D}} = \mathscr{D}\zeta/(cNkT)^2$ during a loading cycle vs maximum strain. The parameters of this network are $p = 5, N = 2$ and $n_t = 1000$.

the inset of panel b. Low and high values of stretch have a lower slope, indicating a smaller predicted change in α. Thus, we see a drop of relaxation as stretches reach moderate to high values. Specifically, the stress relaxes by normalized values of $\Delta\hat{\sigma} = 1.49$ in the first step, $\Delta\hat{\sigma} = 2.51$ in the second step, and $\Delta\hat{\sigma} = 1.67$ in the third step — even though the change in ϵ is the same. Similar stress relaxation experiments were performed by Jiang et al. (2018), but the material was only stretched to a strain of $\epsilon = 6$. As a result, the authors reported a strictly increasing relaxation throughout the experiment. Thus, while our model agrees with these findings, it does predict an inversion of the trend at higher strain.

5.2.2. Little to no energy is dissipated at low values of stretch

To further explore the effect of stretch on network relaxation and dissipation, we now consider a cyclic loading test as studied experimentally by Jiang et al. (2018). In this numerical experiment, the network is again stretched at a constant velocity $\hat{v} = vn_t^2/\xi$ of $\hat{v} = 0.1$ to four distinct strains of $\epsilon = 2, 4, 6$, and 10. After stretching, the network is immediately returned to its original length at the same rate. Fig. 13a&b display normalized α and σ for each of these cases. Also shown are the upper and lower bounds found using Eqs. (50) and (51). The model predicts that little sliding occurs even up to the modest strain of $\epsilon = 6$. This is a combined effect from the smaller stretch-ratio and rate of loading as we will show in the next example. At the largest strain of $\epsilon = 10$, however, there is observable sliding and energy dissipation. This results in a tangible softening of the network and a lower resulting stress (Fig. 13a). These results also align quantitatively with the experimental work by Jiang et al. (2018), who observed little to no hysteresis loop for strains up to $\epsilon = 6$. This can again be explained by the 'S' shaped α curve. Thus, consistently with our previous example, the theory suggests that there is a limit at which the energy dissipation decreases due to the limitations in chain sliding. To confirm this, we calculated the total energy dissipation iteratively using Eq. (46) for the same test, but by varying the strain from 0 and 30. Results in Fig. 13c) show the existence of a linear region between $\epsilon = 10$ and $\epsilon = 20$ in which the energy dissipation per unit strain is optimized. Strains outside of this region suffer from either too little or too much chain reptation as the network is deformed.

5.2.3. Energy dissipation is uniquely dependent on loading rate

In this final example, we explore model predictions regarding the role of loading speed on the energy dissipation of the network. We again use a constant loading velocity, but this time vary the ratio of velocity to friction, causing changes in the activation of the sliding mechanism. Similar to the previous example, the specimen is stretched to a strain $\epsilon = 10$ and then returned to its original length at the same rate. Energy dissipation is calculated incrementally using Eq. (46). We observe similar trends as in the previous example; α increases during deformation and lands on a higher value than that of its resting value (Fig. 14a&b). Subsequently, a visible hysteresis loop is seen in each of the stress–strain curves. Fig. 14a shows the results of a very slow loading speed $\hat{v} = 0.01$, where the network follows a similar equilibrium path to that in Fig. 11. A small level of energy dissipation is observed — we especially note the trend of α as strictly increasing during loading and strictly decreasing during unloading. This means that the

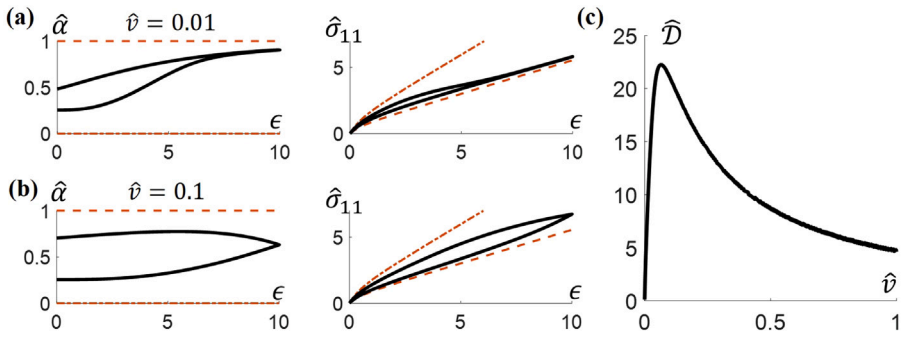

Fig. 14. (a) and (b) Cyclic loading experiment for different loading speeds. The left column is the microscopic response of the network shown by α and the right column is the macroscopic response of the network shown by normalized stress $\sigma/cNkT$. Velocity is normalized as $\hat{v} = vn_l^2/\xi$ to account for variations in the friction parameter, ξ. (c) Normalized energy dissipation, $\hat{\mathcal{D}} = \mathcal{D}\zeta/(cNkT)^2$, exhibited by the network for the same experiment plotted against the normalized velocity. Dashed lines represent the expected response of the network with constant $\hat{\alpha}$ at each of its extremes (corresponding to a full and empty reserve of monomers, respectively.).

network is gaining monomers into its chains during the loading period, which then empty back out as the network returns to its original length. Fig. 14b shows an example of a moderate loading speed of $\hat{v} = 0.1$, where the relaxation time of the network and the rate of deformation are more comparable. Interestingly, we notice an increase in energy dissipation as seen in the large hysteresis loop in the stress–stretch-ratio curve. This is explained by looking again at the sliding profile of α. Specifically, chain sliding does not stop at the end of the loading cycle, rather, α continues to increase even as the network returns back to its original length. This is the result of a slightly higher loading speed causing an offset in the response of the network. Thus, there is a preferred middle-range loading speed where the energy dissipation of the network is maximized. To better understand how loading rate affects network dissipation, we then explored a range of normalized velocities between 0.001 and 1 and calculate the total energy dissipated by the network using Eqs. (50) and (51). Results (depicted in Fig. 14c) clearly show an optimal energy dissipation at approximately $\hat{v} = 0.1$, when the change in α is strictly increasing throughout the duration of the experiment (Fig. 14b).

6. Discussion and concluding remarks

To summarize, slide-ring gels are a very promising class of materials that can be made active through the incorporation of molecular machines (Stoddart, 2017) and could potentially be used as programmable materials in biomedical applications (Bryant and Vernerey, 2018). They also possess a significant energy dissipation potential and unique modes of fracture (Liu et al., 2019a,b) compared to classical gels. Although the above properties are known to be highly dependent on the time-dependence of the gel, existing models (Ito, 2007; Mayumi et al., 2012) have mainly focused on its equilibrium response. In this work, we thus expanded previous work to account for the rate-dependence of these networks. A particularly attractive approach to develop physically meaningful rate-dependent models is the Transient Network Theory (Vernerey et al., 2017; Vernerey, 2018) that has recently been used to describe the mechanics of a wide variety of transient networks from biopolymers (Shen et al., 2019a; Lalitha Sridhar et al., 2018) to active nematic networks (Lalitha Sridhar and Vernerey, 2020; Vernerey et al., 2019, 2018b) including studies on damage and fracture (Shen and Vernerey, 2020; Vernerey et al., 2018a). The main advantage of this theoretical platform is that the model is developed from bottom-up, where the behavior of individual building blocks is first assessed and then assembled into a network model. In the present work, we therefore started from the level of a single chain, with a focus on the interactions between a flexible polymer with mobile and crosslinked rings. We saw here that the roles of the rings were twofold: while crosslinked rings provide topological attachment allowing chain sliding, mobile rings induced an osmotic pressure that fuels the reptation mechanism. The chain model was then used as a stepping stone for the development of a large scale thermodynamically consistent network model. We showed that the dynamics displayed by slide ring networks differ from that of conventional transient networks driven by bond exchange (Lalitha Sridhar and Vernerey, 2018). Indeed, the relaxation mechanism of slide rings is limited to one degree of freedom in the form of monomers sliding into and out of the elastic segments. This imposes physical restrictions onto the degree of network relaxation, captured here by an internal state variable α representing the amount of chain sliding. The sliding was particularly found to be constrained within two bounds on which the network's response returns to that of a covalently bonded network. The transition between these two states was quantified by developing a Fokker–Planck equation for the network and illustrated by an incremental solving scheme.

The proposed model addresses a number of questions posed by researchers (Ito, 2007; Kato et al., 2014, 2015; Mayumi et al., 2012). At the level of a single chain, we provided rational explanations for the molecular parameters that govern the behavior of polyrotaxane, that could later be used to assist in the design of slide ring gels with tunable relaxation times and stiffnesses. At the network level, the model could reproduce and explain current experimental results on the stress relaxation and cyclic response of slide-ring gels. A key assumption of the model is the affine kinematics of the crosslinks, but not the chains. Many present-day polymer models (Treloar, 1943; James, 1947) indeed rely on treating individual chains of the network as if they were rigidly attached to an elastic background. The chains are then assumed to be stretched by the same macroscopic deformation of the body. Our definition

of affine deformation differs slightly from this view; we treat individual chains of polyrotaxane as being attached to the elastic background by their crosslinked mobile rings. Thus, the polymer chain whose elasticity is responsible for the stress response of the network is not assumed to be attached to the elastic background. Rather, the chain is assumed to slide within the rigidly attached mobile rings as the network deforms. The crosslinked rings are then assumed to be deformed affinely in our model. An alternative view would be to assume that the polymer chains are static, and the mobile rings present along the chain slide along the chain as is commonly cited in the literature (Okumura and Ito, 2001). We note that from the standpoint of a continuum-level description of the network, these two views are the same; the relative motion of mobile rings to polymer chains is captured with either viewpoint.

For the clarity of the presentation, the proposed framework remains in its minimal form and is therefore subject to a number of limitations. Notably, many of the tensile tests performed on slide ring gels result in an 'S' shaped curve (Jiang et al., 2018). While our model captures the initial softening of the network, it fails to stiffen at higher deformation. The reason for this stiffening is classically attributed to the stiffening of the chains as they approach their contour-length (Doi, 2013), a feature that is not captured by the Gaussian formulation used in our study. To address this shortcoming, the free energy of flexible chains would need to be based on the Langevin function (Liu and Muthukumar, 1998), which can be naturally incorporated within the framework of the TNT (Vernerey, 2018). Another potential limitation is the phenomenological nature of the friction coefficient ξ, which governs the relaxation time. Indeed, we saw in Section 2 that the relaxation time of a single chain was nonlinearly dependent on molecular design, i.e. N, P and n_t. While the determination of a closed-form relationship was however beyond the scope of this study, such an enterprise will only be successful if performed in concert with an experimental component. Furthermore, before it can be used as a design tool, the proposed model will need to incorporate additional physical features such as alternative rate-dependent processes (chain diffusion via the Rouse model (Doi, 2013), or chain entanglements (Ball et al., 1981)), or even polydiverse networks. All of these improvements would predict a wider range of relaxation magnitude and timescales that could realistically predict experimental work. The implementation of such models within a finite-element formulation (Shen et al., 2019b; Foucard et al., 2015) will finally be essential in understanding the role of non-uniform deformations and boundary conditions in the response of these gels.

CRediT authorship contribution statement

Franck J. Vernerey: Conceptualization, Methodology, Writing - original draft, Supervision. **Samuel Lamont:** Software, investigation, Writing - review & editing, Visualization.

Declaration of competing interest

The authors declare that they have no known competing financial interests or personal relationships that could have appeared to influence the work reported in this paper.

Acknowledgments

FJV gratefully acknowledges the support of the National Science Foundation, USA under award no. 2023179 . The content is solely the responsibility of the authors and does not necessarily represent the official views of the University of Colorado Boulder or the National Science Foundation.

References

Ball, R.C., Doi, M., Edwards, S.F., Warner, M., 1981. Elasticity of entangled networks. Polymer 22 (8), 1010–1018.
Baulin, Vladimir A., Johner, Albert, Marques, Carlos M., 2005. Sliding grafted polymer layers. Macromolecules 38 (4), 1434–1441.
Bitoh, Yohsuke, Akuzawa, Norio, Urayama, Kenji, Takigawa, Toshikazu, Kidowaki, Masatoshi, Ito, Kohzo, 2011. Peculiar nonlinear elasticity of polyrotaxane gels with Movable cross-links revealed by multiaxial stretching. Macromolecules 44 (21), 8661–8667.
Boesten, Ruud J.J., Sevick, Edith M., Williams, David R.M., 2010. Piston rotaxane monolayers: Shear swelling and nanovalve behavior. Macromolecules 43 (17), 7244–7249.
Bryant, Stephanie J., Vernerey, Franck J., 2018. Programmable hydrogels for cell encapsulation and Neo-tissue growth to enable personalized tissue engineering. Adv. Healthc. Mater. 7 (1), n/a–n/a.
de Gennes, P.G., Leger, L., 1982. Dynamics of entangled polymer chains. Annu. Rev. Phys. Chem. 33 (1), 49–61.
Doi, Masao, 2013. Soft Matter Physics. OUP Oxford, Google-Books-ID: ccUaBj73PZsC.
Doi, Masao, Edwards, S.F., 1978a. Dynamics of concentrated polymer systems. Part 1.–Brownian motion in the equilibrium state. J. Chem. Soc. Faraday Trans. 2: Mol. Chem. Phys. 74, 1789–1801.
Doi, Masao, Edwards, S.F., 1978b. Dynamics of concentrated polymer systems. Part 3.–The constitutive equation. J. Chem. Soc. Faraday Trans. 2: Mol. Chem Phys. 74, 1818–1832.
Edwards, S.F., 1967. The statistical mechanics of polymerized material. Proc. Phys. Soc. 92 (1), 9–16.
Feringa, Ben L., 2017. The art of building small: From molecular switches to motors (Nobel Lecture). Angew. Chem. Int. Ed. 56 (37), 11060–11078, _eprint: https://onlinelibrary.wiley.com/doi/pdf/10.1002/anie.201702979.
Flory, Paul J., Rehner, John, 1943. Statistical mechanics of cross–linked polymer networks I. rubberlike elasticity. J. Chem. Phys. 11 (11), 512–520.
Foucard, Louis, Aryal, Anup, Duddu, Ravindra, Vernerey, Franck, 2015. A coupled Eulerian–Lagrangian extended finite element formulation for simulating large deformations in hyperelastic media with moving free boundaries. Comput. Methods Appl. Mech. Engrg. 283, 280–302.
Goujon, Antoine, Lang, Thomas, Mariani, Giacomo, Moulin, Emilie, Fuks, Gad, Raya, Jesus, Buhler, Eric, Giuseppone, Nicolas, 2017. Bistable [c2] daisy chain rotaxanes as reversible muscle-like Actuators in mechanically active gels. J. Am. Chem. Soc. 139 (42), 14825–14828.
Hashidzume, Akihito, Yamaguchi, Hiroyasu, Harada, Akira, 2019. Cyclodextrin-based rotaxanes: from rotaxanes to polyrotaxanes and further to functional materials. Eur. J. Org. Chem. 2019 (21), 3344–3357.

Ito, Kohzo, 2007. Novel cross-linking concept of polymer network: Synthesis, structure, and properties of slide-ring gels with freely movable junctions. Polym. J. 39 (6), 489–499.
Ito, Kohzo, 2012. Novel entropic elasticity of polymeric materials: why is slide-ring gel so soft? Polym. J. 44 (1), 38–41.
James, Hubert M., 1947. Statistical properties of networks of flexible chains. J. Chem. Phys. 15 (9), 651–668.
James, Hubert M., Guth, Eugene, 1943. Theory of the elastic properties of rubber. J. Chem. Phys. 11 (10), 455–481.
Jiang, Lan, Liu, Chang, Mayumi, Koichi, Kato, Kazuaki, Yokoyama, Hideaki, Ito, Kohzo, 2018. Highly stretchable and instantly recoverable slide-ring gels consisting of enzymatically synthesized polyrotaxane with low host coverage. Chem. Mater. 30 (15), 5013–5019, Publisher: American Chemical Society.
Kato, Kazuaki, Okabe, Yoshinori, Okazumi, Yuya, Ito, Kohzo, 2015. A significant impact of host–guest stoichiometry on the extensibility of polyrotaxane gels. Chem. Commun. 51 (90), 16180–16183.
Kato, Kazuaki, Yasuda, Takaaki, Ito, Kohzo, 2013. Viscoelastic properties of slide-ring gels reflecting sliding dynamics of partial chains and entropy of ring components. Macromolecules 46 (1), 310–316.
Kato, Kazuaki, Yasuda, Takaaki, Ito, Kohzo, 2014. Peculiar elasticity and strain hardening attributable to counteracting entropy of chain and ring in slide-ring gels. Polymer 55 (10), 2614–2619.
Kuhn, Werner, 1946. Dependence of the average transversal on the longitudinal dimensions of statistical coils formed by chain molecules. J. Polym. Sci. 1 (5), 380–388.
Lalitha Sridhar, Shankar, Ortega, Joseph K.E., Vernerey, Franck J., 2018. A statistical model of expansive growth in plant and fungal cells: The case of phycomyces. Biophys. J. 115 (12), 2428–2442.
Lalitha Sridhar, Shankar, Vernerey, Franck J., 2018. The chain distribution tensor: Linking nonlinear rheology and chain anisotropy in transient polymers. Polymers 10 (8), 848, Publisher: MDPI.
Lalitha Sridhar, Shankar, Vernerey, Franck J., 2020. Mechanics of transiently cross-linked nematic networks. J. Mech. Phys. Solids 141, 104021.
Liu, Chang, Kadono, Hirokazu, Mayumi, Koichi, Kato, Kazuaki, Yokoyama, Hideaki, Ito, Kohzo, 2017. Unusual fracture behavior of slide-ring gels with movable cross-links. ACS Macro Lett. 6 (12), 1409–1413.
Liu, Chang, Kadono, Hirokazu, Yokoyama, Hideaki, Mayumi, Koichi, Ito, Kohzo, 2019a. Crack propagation resistance of slide-ring gels. Polymer 181, 121782.
Liu, Chang, Mayumi, Koichi, Hayashi, Kyohei, Jiang, Lan, Yokoyama, Hideaki, Ito, Kohzo, 2019b. Direct observation of large deformation and fracture behavior at the crack tip of slide-ring gel. J. Electrochem. Soc. 166 (9), B3143–B3147.
Liu, C., Muthukumar, M., 1998. Langevin dynamics simulations of early-stage polymer nucleation and crystallization. J. Chem. Phys. 109 (6), 2536–2542, Publisher: American Institute of Physics.
Mayumi, Koichi, Tezuka, Masahiko, Bando, Akinori, Ito, Kohzo, 2012. Mechanics of slide-ring gels: novel entropic elasticity of a topological network formed by ring and string. Soft Matter 8 (31), 8179–8183.
Noda, Yumiki, Hayashi, Yuki, Ito, Kohzo, 2014. From topological gels to slide-ring materials. J. Appl. Polym. Sci. 131 (15).
Okumura, Y., Ito, K., 2001. The polyrotaxane gel: A topological gel by Figure-of-eight cross-links. Adv. Mater. 13 (7), 485–487.
Pinson, Matthew B., Sevick, Edith M., Williams, David R.M., 2013. Mobile rings on a polyrotaxane lead to a yield force. Macromolecules 46 (10), 4191–4197.
Rubinstein, Michael, Panyukov, Sergei, 1997. Nonaffine deformation and elasticity of polymer networks. Macromolecules 30 (25), 8036–8044.
Rubinstein, Michael, Panyukov, Sergei, 2002. Elasticity of polymer networks. Macromolecules 35 (17), 6670–6686.
Sauvage, Jean-Pierre, 2017. From chemical topology to molecular machines (nobel lecture). Angew. Chem. Int. Ed. 56 (37), 11080–11093, _eprint: https://onlinelibrary.wiley.com/doi/pdf/10.1002/anie.201702992.
Sevick, E.M., Williams, D.R.M., 2010. Piston-rotaxanes as molecular shock absorbers. Langmuir 26 (8), 5864–5868.
Shen, Tong, Benet, Eduard, Sridhar, Shankar Lalitha, Abadie, Joel, Piat, Emmanuel, Vernerey, Franck J., 2019a. Separating the contributions of zona pellucida and cytoplasm in the viscoelastic response of human oocytes. Acta Biomater. 85, 253–262.
Shen, Tong, Long, Rong, Vernerey, Franck, 2019b. Computational modeling of the large deformation and flow of viscoelastic polymers. Comput. Mech. 63 (4), 725–745.
Shen, Tong, Vernerey, Franck J., 2020. Rate-dependent fracture in transient networks. J. Mech. Phys. Solids 104028.
Stoddart, J. Fraser, 2017. Mechanically interlocked molecules (MIMs)—Molecular shuttles, switches, and machines (Nobel Lecture). Angew. Chem. Int. Ed. 56 (37), 11094–11125, _eprint: https://onlinelibrary.wiley.com/doi/pdf/10.1002/anie.201703216.
Tanaka, F., Edwards, S.F., 1992. Viscoelastic properties of physically crosslinked networks. 1. transient network theory. Macromolecules 25 (5), 1516–1523.
Treloar, L.R.G., 1943. The elasticity of a network of long-chain molecules—II. Trans. Faraday Soc. 39, 241–246.
Vernerey, Franck J., 2018. Transient response of nonlinear polymer networks: A kinetic theory. J. Mech. Phys. Solids 115, 230–247.
Vernerey, F.J., Benet, E., Blue, L., Fajrial, A.K., Lalitha Sridhar, S., Lum, J.S., Shakya, G., Song, K.H., Thomas, A.N., Borden, M.A., 2019. Biological active matter aggregates: Inspiration for smart colloidal materials. Adv. Colloid Interface Sci. 263, 38–51.
Vernerey, Franck J., Brighenti, Roberto, Long, Rong, Shen, Tong, 2018a. Statistical damage mechanics of polymer networks. Macromolecules 51 (17), 6609–6622.
Vernerey, Franck J., Long, Rong, Brighenti, Roberto, 2017. A statistically-based continuum theory for polymers with transient networks. J. Mech. Phys. Solids 107, 1–20.
Vernerey, Franck J., Shen, Tong, Sridhar, Shankar Lalitha, Wagner, Robert J., 2018b. How do fire ants control the rheology of their aggregations? A statistical mechanics approach. J. R. Soc. Interface 15 (147), 20180642, Publisher: Royal Society.